The protective effect of A20 on atherosclerosis in apolipoprotein E-deficient mice is associated with reduced expression of NF-κB target genes

Susanne Wolfrum*, Daniel Teupser*†, Marietta Tan*, Kwan Y. Chen*, and Jan L. Breslow*‡

*Laboratory of Biochemical Genetics and Metabolism, The Rockefeller University, New York, NY 10065; and †Institute of Laboratory Medicine, Clinical Chemistry, and Molecular Diagnostics, University of Leipzig, 04103 Leipiz, Germany

Contributed by Jan L. Breslow, September 21, 2007 (sent for review September 7, 2007)

Up-regulation of inflammatory responses is considered a driving force of atherosclerotic lesion development. One key regulator of inflammation is the A20 (also called TNF-α-induced protein 3 or Tnfaip3) gene, which is responsible for NF-κB termination and maps to an atherosclerosis susceptibility locus revealed by quantitative trait locus-mapping studies at mouse proximal chromosome 10. In the current study, we examined the role of A20 in atherosclerotic lesion development. At the aortic root lesion size was found to be increased in C57BL/6 (BG) apolipoprotein E-deficient (ApoE$^{-/-}$) mice haploinsufficient for A20, compared with B6 ApoE$^{-/-}$ controls that expressed A20 normally (60% in males and 23% in females; $P < 0.001$ and $P < 0.05$, respectively). In contrast, lesion size was found to be decreased in F_1 (B6×FVB/N) mice overexpressing A20 by virtue of containing an A20 BAC transgene compared with nontransgenic controls (30% in males, $P < 0.001$, and 17% in females, $P = 0.02$). The increase in lesions in the A20 haploinsufficient mice correlated with increased expression of proatherosclerotic NF-κB target genes, such as vascular cell adhesion molecule 1, intercellular adhesion molecule 1, and macrophage-colony-stimulating factor, and elevated plasma levels of NF-κB-driven cytokines. These findings suggest that A20 diminishes atherosclerosis by decreasing NF-κB activity, thereby modulating the proinflammatory state associated with lesion development.

Atherosclerosis is a chronic inflammatory disease influenced by many genes, and mouse models are useful for identifying these genes and determining their mechanisms of action. We previously carried out an intercrosses between atherosclerosis-sensitive apolipoprotein E-deficient (ApoE$^{-/-}$) C57BL/6 (B6) and atherosclerosis-resistant ApoE$^{-/-}$ FVB mice, and by quantitative trait locus mapping identified an atherosclerosis-susceptibility locus on proximal chromosome 10 (1, 2). A candidate gene in this region, A20, encodes a broadly expressed cytoplasmic protein that inhibits both TNF-α- and IL-1β/Toll-like receptor (TLR)-induced NF-κB activation through mediating the destruction of receptor-interacting serine/threonine protein kinase 1 (RIP) and TNF receptor-associated factor 6 in their respective signaling complexes (3, 4). Up-regulation of NF-κB activity leads to increased expression of many genes with established roles in atherosclerosis, including cytokines, chemokines, adhesion molecules, acute phase proteins, and regulators of apoptosis and cell proliferation. NF-κB terminates its own activation by inducing the expression of IκBα and A20. A20-deficient (A20$^{-/-}$) mice die prematurely because of cachexia and spontaneous inflammation in several organs. This phenotype correlates with the failure to properly terminate TNF-induced NF-κB activity in fibroblasts isolated from A20$^{-/-}$ mice (5). We previously determined that A20 derived from B6 and FVB mice differs in a single amino acid residue (E627A; B6 vs. FVB). We showed this finding to be functionally significant by demonstrating that the B6 form compared with the FVB form was less effective in terminating TNF-α induced NF-κB activity. Compatible with this finding, we also showed that TNF-α induced expression of the NF-κB target genes A20 and IκBα was prolonged in vascular smooth muscle cells isolated from B6 compared with FVB mice (6).

The aim of the current study was to determine whether A20 can directly influence atherosclerosis susceptibility. To this end, we compared ApoE$^{-/-}$ mice that express A20 normally with those that are haploinsufficient for A20 or those that carry an A20 BAC transgene. Our results indicate that mice haploinsufficient for A20 develop larger lesions associated with increased expression of the NF-κB target genes vascular cell adhesion molecule 1 (VCAM-1), intercellular adhesion molecule 1 (ICAM-1), and macrophage-colony-stimulating factor (M-CSF), and increased plasma levels of NF-κB-regulated cytokines. In contrast, A20 BAC transgenic (tg) overexpression of A20 results in smaller lesions. These results strongly suggest that A20, acting mainly through effects mediated by NF-κB, can influence atherosclerosis susceptibility.

Results

Atherosclerosis Is Increased in A20 Haploinsufficient and Decreased in A20 Overexpressing Mice. Atherosclerosis was compared between B6.ApoE$^{-/-}$.A20$^{+/+}$ and B6.ApoE$^{-/-}$.A20$^{+/-}$ littermate controls, and, as shown in Fig. 1*A*, A20 haploinsufficiency increased mean aortic root lesion area by 60% ($P < 0.001$) in males and 23% ($P < 0.05$) in females. Lesion area differences between the genotypes were not explained by differences in total or high-density lipoprotein cholesterol levels. Atherosclerosis was also compared between F_1 ApoE$^{-/-}$ mice with and without the A20 transgene, and, as shown in Fig. 1*B*, the A20 BAC transgene decreased mean aortic root lesion area by 30% ($P < 0.001$) in males and 17% ($P = 0.02$) in females. Lesion area differences were smaller in females in both the haploinsufficiency and overexpression studies, which could hint toward a gender difference or be the consequence of the fact that differences in lesion size become less prominent the larger the lesions. Lesion area differences between the genotypes were not explained by differences in total or high-density lipoprotein cholesterol levels. Thus it appears that A20 underexpression increases and A20 overexpression decreases atherosclerosis susceptibility.

Author contributions: J.L.B. designed research; S.W., D.T., M.T., and K.Y.C. performed research; and S.W. and J.L.B. wrote the paper.

The authors declare no conflict of interest.

Freely available online through the PNAS open access option.

Abbreviations: ApoE$^{-/-}$, apolipoprotein E-deficient; B6, C57BL/6; TLR, Toll-like receptor; VCAM-1, vascular cell adhesion molecule 1; ICAM-1, intercellular adhesion molecule 1; M-CSF, macrophage-colony-stimulating factor; tg, transgenic; ST, soluble transducer; AKAP-1, A-kinase anchor protein 1; Myd88, myeloid differentiation factor 88; CAD, coronary artery disease; RIP, receptor-interacting serine/threonine protein kinase 1.

‡To whom correspondence should be addressed. E-mail: breslow@rockefeller.edu.

This article contains supporting information online at www.pnas.org/cgi/content/full/0709011104/DC1.

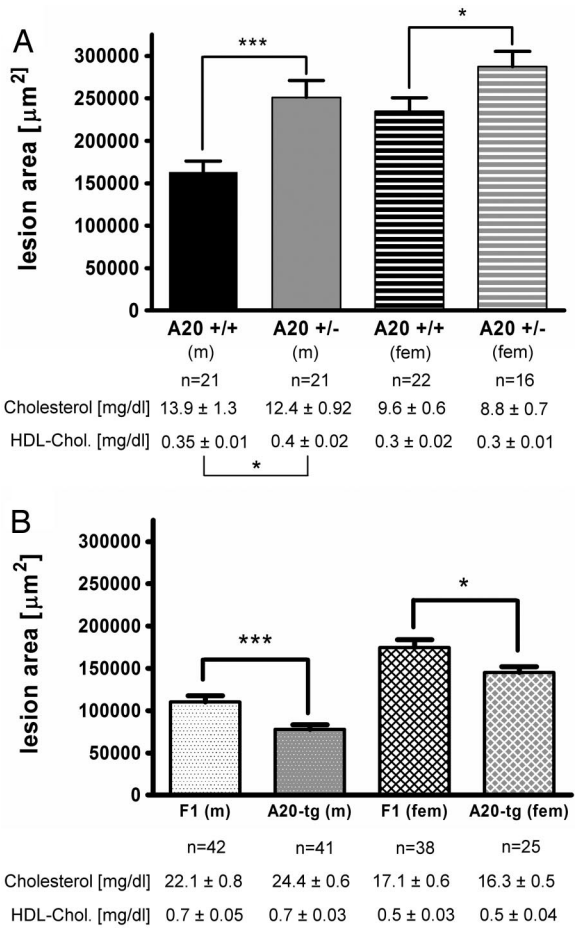

Fig. 1. Aortic root lesion area and plasma cholesterol levels in ApoE$^{-/-}$ mice at 16 weeks of age after administration of a semisynthetic 0.02% cholesterol diet for 12 weeks. (*A*) Male (m) and female (fem) A20$^{+/+}$ and A20$^{+/-}$ mice on the B6 background. (*B*) Male (m) and female (fem) tg(A20) and control mice on an F_1 (B6xFVB) background. Bars represent means ± SEM, and the numbers of animals in the individual groups are given underneath the bars. *, $P \leq 0.05$; **, $P \leq 0.01$; ***, $P \leq 0.001$.

Morphology of Aortic Root Lesions in A20 Haploinsufficient Mice. Lesion morphology was assessed in frozen aortic root sections of B6.ApoE$^{-/-}$ A20$^{+/+}$ and B6.ApoE$^{-/-}$A20$^{+/-}$ mice. In general, lesions of both genotypes were quite similar and consisted mainly of foam cells with occasional cholesterol clefts and/or necrotic areas and beginning fibrous caps (Fig. 2*A*). However, at higher power (Fig. 2*B*) ≈50% of the lesions from the A20 haploinsufficient mice appeared to contain a white cell infiltrate throughout the plaque, not seen in sections from A20$^{+/+}$ mice. This observation suggests that A20 haploinsufficiency promotes a proinflammatory phenotype in the arterial wall of atherosclerosis–prone mice and might in this manner accelerate lesion progression. White blood cell infiltration (granulocytes, lymphocytes, and macrophages) has been previously reported in various tissues in A20$^{-/-}$ mice, and it appeared that granulocytes and/or macrophages were more to blame for the inflammatory state than were lymphocytes (5, 7). Lesions were also stained for A20 (Fig. 2*C*), endothelial cells (CD-31; Fig. 2*D*), macrophages (CD68; Fig. 2*E*), and smooth muscle cells (α-actin; Fig. 2*F*). These stains demonstrated that A20 is present in atherosclerotic lesions and colocalizes mainly with macrophages and endothelial cells. However, the aortic root lesions of A20$^{+/+}$ and A20$^{+/-}$ mice showed the same A20 cell-type specific expression pattern as well as an apparent amount of A20 expression (comparison not shown). The TUNEL method was used to visualize apoptotic cells and revealed apoptosis to be present (Fig. 2*G*) in macrophage-rich regions (Fig. 2*H*). No apparent difference in the amount of macrophage apoptosis was found between B6.ApoE$^{-/-}$A20$^{+/+}$ and B6.ApoE$^{-/-}$A20$^{+/-}$ mice.

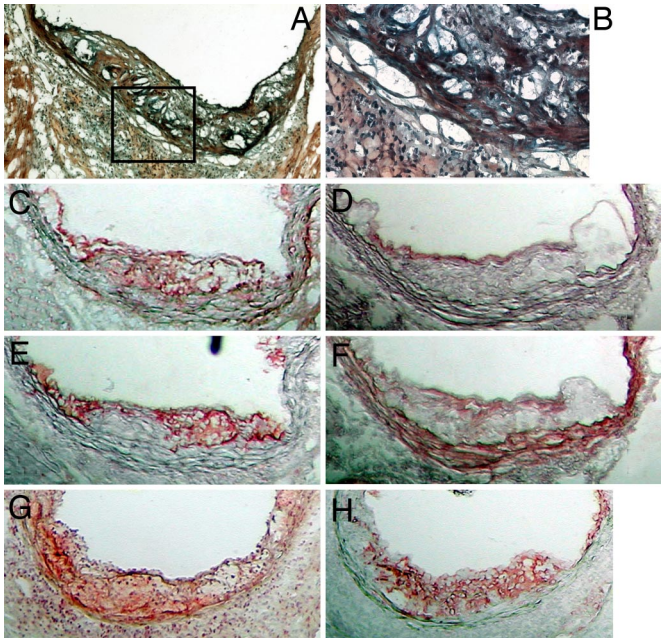

Fig. 2. Frozen aortic root sections at 16 weeks of age. (*A*) Movats stain of a B6.ApoE$^{-/-}$.A20$^{+/-}$ mouse. (*B*) Higher-power view of the boxed area of *A* representing an area of a white cell infiltrate. (*C–F*) Serial sections stained for A20 (red) (*C*), CD31 (red) (*D*), CD68 (red) (*E*), and α-actin (red) (*F*). (*G* and *H*) Other representative serial sections were stained for TUNEL (red) (*G*) and CD68 (red) (*H*). (Magnification: *A*, ×100; *B*, ×400; *C–H*, ×100.)

A20 Haploinsufficiency Results in Altered Expression of NF-κB-Related Genes. As shown in Fig. 3, the livers of A20-haploinsufficient mice had ≈50% of normal A20 mRNA levels, and, presumably as a consequence, mRNA levels of several NF-κB target genes

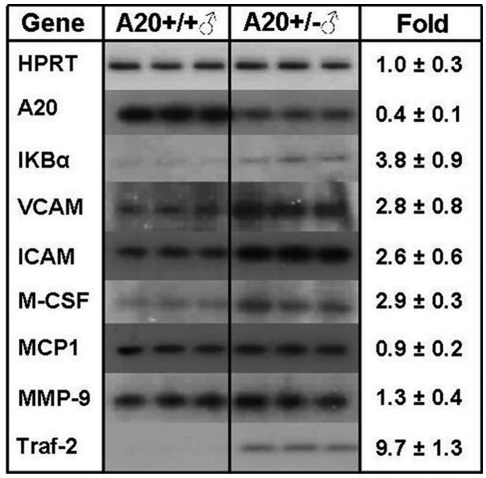

Fig. 3. Expression of NF-κB-related genes in liver in male B6.ApoE$^{-/-}$.A20$^{+/+}$ (*Left*) and A20$^{+/-}$ (*Right*) mice at 16 weeks of age. Expression levels were measured by RT-PCR with hypoxanthine phosphoribosyltransferase (HPRT) as a control. MCP-1, monocyte chemoattractant protein 1; MMP-9, matrix metalloproteinase type 9.

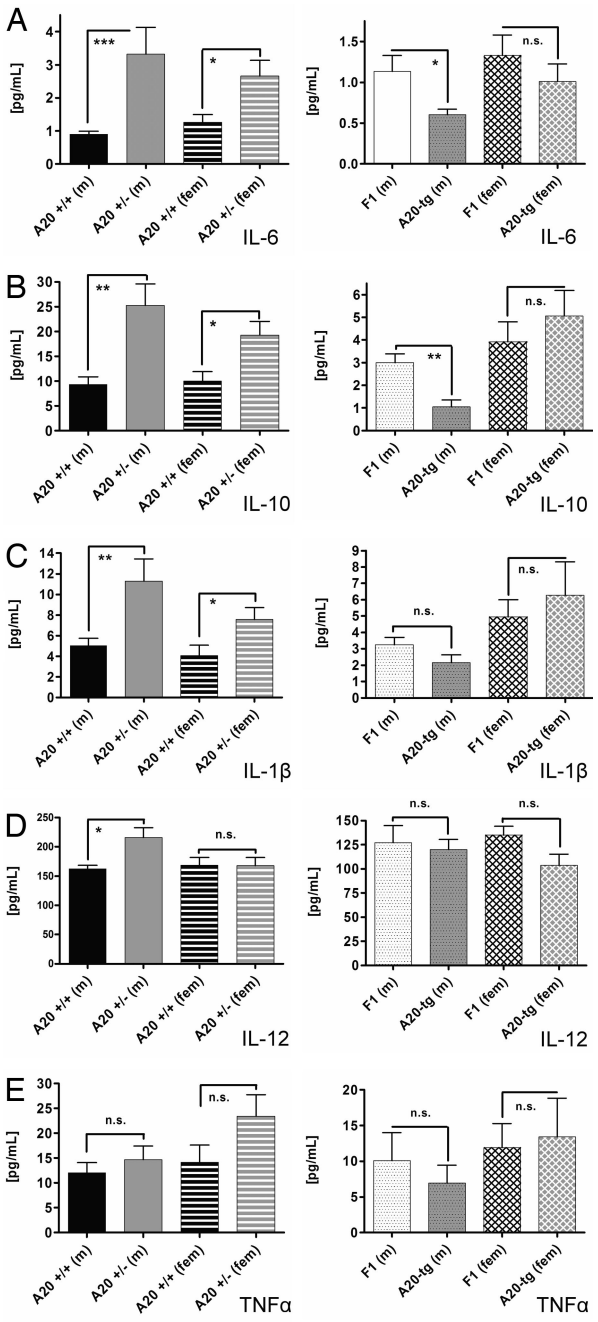

Fig. 4. Plasma levels of NF-κB-regulated cytokines were determined by a multiplex suspension ELISA in male (m) and female (fem) B6.ApoE$^{-/-}$.A20$^{+/+}$ and A20$^{+/-}$ mice (*Left*) and in F_1 ApoE$^{-/-}$ tg(A20) and F_1 ApoE$^{-/-}$ control mice (*Right*). (*A*) IL-6 levels. (*B*) IL-10 levels. (*C*) IL-1β levels. (*D*) IL-12 levels. (*E*) TNF-α-levels. $n = 10$ in each group. Means and SEM are shown. *, $P \leq 0.05$; **, $P \leq 0.01$; ***, $P \leq 0.001$.

were increased, including IκBα (3.8 ± 0.9-fold), VCAM-1 (2.8 ± 0.8-fold), ICAM-1 (2.6 ± 0.6-fold), and M-CSF (2.9 ± 0.3-fold). mRNA levels for monocyte chemoattractant protein 1 (MCP-1) (0.9 ± 0.2 fold) and matrix metalloproteinase type 9 (1.3 ± 0.4-fold) were unchanged, whereas expression of the NF-κB activation mediator TRAF-2 was highly increased (9.7 ± 1.3-fold). Thus, A20-haploinsufficient mice fail to produce sufficient A20 to adequately shut off endogenous NF-κB activation, which results in increased expression of several proatherosclerotic NF-κB target genes.

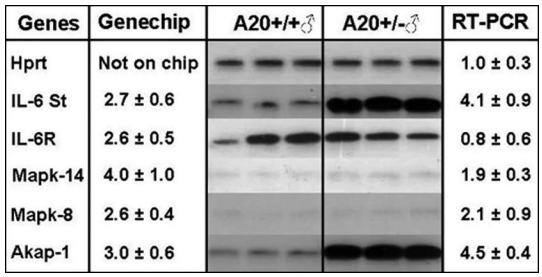

Fig. 5. Genes differentially expressed on a PIQOR immunology, mouse-sense microarray in liver at 16 weeks of age between male B6.ApoE$^{-/-}$.A20$^{+/+}$ and A20$^{+/-}$ mice with confirmation by RT-PCR. Hypoxanthine phosphoribosyltransferase (Hprt) served as a control. Fold induction found for each gene in the microarray and by RT-PCR are shown.

A20 Haploinsufficiency and Expression of an A20 Transgene Affect Plasma Levels of NF-κB-Regulated Cytokines. Fig. 4 *A* and *B* shows plasma levels of IL-6 and IL-10 increased in male and female A20-haploinsufficient mice and decreased in male and unchanged in female tg(A20) mice. Fig. 4*C* shows plasma levels of IL-1β were increased in male and female A20-haploinsufficient mice, but not significantly changed in male and female tg(A20) mice. Fig. 4*D* shows plasma levels of IL-12 (p40) were increased in male A20-haploinsufficient mice but unchanged in females and male and female tg(A20) mice. Fig. 4*E* shows plasma levels of TNF-α trended toward increased levels in haploinsufficient mice and reduced levels in tg(A20) mice (not statistically significant). Thus, in general, A20 haploinsufficiency resulted in up-regulation of NF-κB-regulated cytokines, whereas the opposite occurred in tg(A20) mice. This result is compatible with increased atherosclerosis in the former and decreased atherosclerosis in the latter.

Other Potential Pathways by Which A20 Might Influence the Development of Atherosclerosis. As shown in Fig. 5, liver gene expression patterns showed that A20-haploinsufficient mice had increased expression of IL-6 soluble transducer (ST), also named gp130. This increase could result in activation of the IL-6 pathway even though expression of the IL-6 receptor itself was not regulated. Also shown in Fig. 5, A20-haploinsufficient mice had increased expression of the MAP kinases, p38 (MAPK-14) and JNK (MAPK-8) (both ≈2-fold by RT-PCR), and both of these MAP kinases can stimulate the expression of proinflammatory genes (8). BecauseTRAF-2 activates the MAP kinases p38 and JNK, the increase in TRAF-2 expression in A20-haploinsufficient mice (Fig. 3) is probably responsible for increased p38 and JNK expression. Finally, Fig. 5 shows that the A-kinase anchor protein 1 (AKAP-1) was up-regulated (4.5 ± 0.4-fold by RT-PCR) in A20-haploinsufficient mice. AKAP-1 localizes PKA activity by binding to the PKA regulatory subunit, and thereby confining expression to either the mitochondria or the endoplasmic reticulum depending on the N-terminal part of the AKAP-1 protein, which differs between splice variants. Thus, A20, in addition to regulating the NF-κB pathway, may also alter atherosclerosis susceptibility through effects on other pathways, such as IL-6 via IL-6-ST, MAP kinases involving p38 and JNK, and PKA by affecting intracellular locations.

Discussion

In this article, A20, a potent physiological inhibitor of the NF-κB pathway, has been shown to affect atherosclerosis susceptibility. In the ApoE$^{-/-}$ mouse model A20 haploinsufficiency was found to increase and A20 overexpression via transgenesis was found to decrease aortic root atherosclerotic lesion area. A20 was shown by immunohistochemical staining to be present in lesions

primarily in endothelial cells and lipid-laden macrophages. Microscopic pathological examination of atherosclerotic lesions also revealed the frequent presence of a white cell infiltrate in lesions from B6.ApoE$^{-/-}$.A20$^{+/-}$ mice. A20 haploinsufficiency resulted in increased liver expression of several NF-κB-regulated genes linked to increased atherosclerosis, including VCAM, ICAM-1, and M-CSF. Moreover, A20 haploinsufficiency and expression of an A20 transgene altered the plasma levels of several atherosclerosis-related NF-κB-regulated cytokines. In addition, A20 haploinsufficiency affected other signaling pathways that could play a role in atherogenesis, such as IL-6, MAP kinases, and PKA. Thus, a number of pathways might contribute to the effects of varying A20 expression on atherosclerosis susceptibility.

NF-κB is active in lesion-prone regions, and NF-κB-regulated genes play major roles in lesion initiation. It is therefore logical that A20 influences atherogenesis by regulating NF-κB activation. For example, in lesion-prone regions an early endothelial cell surface change is the appearance of VCAM-1 (9–11). VCAM-1 recognizes VLA4 on the surface of monocytes. This interaction allows the firm attachment required before entry of monocytes into the subendothelial space. Highlighting the importance of VCAM-1 in lesion formation are the findings that VCAM-1 hypomorphic mice expressing very low levels of VCAM-1 have dramatically decreased aortic root lesion area on both the ApoE$^{-/-}$ and low-density lipoprotein receptor (LDLR)$^{-/-}$ backgrounds (12, 13). The VCAM-1 gene has two NF-κB response elements in its promoter previously shown to be required for cytokine-induced VCAM-1 expression in endothelial cells, smooth muscle cells, and some nonvascular cells. In the current study, A20 haploinsufficiency leading to prolonged NF-κB expression was the likely proximate cause of the 2.8-fold increase in VCAM-1 mRNA levels found in liver, but also presumably present in cells of lesion prone sites of the vasculature. In another example, after monocytes enter the subendothelial space they differentiate into lesional macrophages. This step is mediated by another NF-κB-regulated gene M-CSF (14), whose relevance for lesion formation was shown in mouse atherosclerosis models in which virtually no lesions developed in the absence of M-CSF (15, 16). In the current study, M-CSF mRNA levels were up-regulated 2.9-fold in liver from A20-haploinsufficient mice, which also presumably reflects the cells of the vasculature. Thus, A20-haploinsufficient mice may have increased atherosclerosis through prolonged NF-κB activation, causing increased endothelial-leukocyte adhesion (VCAM-1) and monocyte to macrophage differentiation (M-CSF) at lesion-prone sites.

NF-kB activation can occur via several distinct pathways; two of these are TNF-α and IL-1/TLR signaling. These pathways merge at the level of IκB kinase (IKK) complex activation. TNF-α is considered a proinflammatory cytokine and transduces its signal upon binding to two different receptors (p55 and p75). Although TNF-α was hypothesized to play a major role in atherogenesis, studies using mouse models deficient in TNF-α or one of its receptors have given confusing results. Whereas the absence of receptor p75 did not appear to affect atherosclerosis, deficiency of receptor p55 actually increased lesion formation 2- to 3-fold (17). A subsequent study found that TNF-α deficiency on the ApoE$^{-/-}$ background decreased atherosclerosis (35–50%), as originally expected (18, 19). In the current study, we found A20-haploinsufficient mice to have unchanged circulating levels of TNF-α, which suggests that half-normal A20 production is capable of regulating NF-κB-driven TNF-α production, although other explanations are possible. Thus, it appears that circulating levels of TNF-α, if they are important at all in promoting atherosclerotic lesion development, are not the driving force behind the increased atherosclerosis in A20-haploinsufficient mice.

A second signaling pathway that can activate NF-κB involves many receptors, including receptors for IL-1β and IL-18, and TLRs. All of these receptors signal through myeloid differentiation factor 88 (Myd88) and TRAF-6. The role of the proinflammatory cytokine IL-1β has been studied in mouse atherosclerosis models by using both IL-1β and IL-1β receptor-deficient mice. The absence of IL-1β in ApoE$^{-/-}$ mice decreased atherosclerosis ≈30%, which was accompanied by a decrease in VCAM-1 and MCP-1 (20). Concordantly, IL-1β receptor deficiency on the ApoE$^{-/-}$ background decreased atherosclerosis (21). Interestingly, in the current study, A20-haploinsufficient mice had increased circulating levels of the NF-κB-regulated cytokine IL-1β, which could contribute to enhanced lesion development in these mice. In other studies, IL-18 deficiency in ApoE$^{-/-}$ mice diminished atherosclerosis development, and in two studies Myd88 deficiency in ApoE$^{-/-}$ mice markedly diminished atherosclerosis (60%). Finally, TLR2 and TLR4 deficiency on the ApoE$^{-/-}$ background was also shown to decrease atherosclerosis (22, 23). Thus, it appears that blocking the route of NF-κB activation that involves Myd88 and TRAF-6 is consistently antiatherogenic (22, 24). These results in the context of the current study suggest that the atheroprotective effect of A20 is most likely caused by its ability to shut down NF-κB activation via the Myd88–TRAF-6 signaling pathway through its ability to mediate the degradation of TRAF-6, rather than terminating TNF-induced NF-κB activation by mediating degradation of RIP.

It is possible that altered A20 expression might influence atherosclerosis susceptibility by regulating other pathways, such as those mediated by IL-6, MAP kinases, and PKA. The effect of IL-6 on atherosclerosis is unclear; whereas administration of recombinant IL-6 increased atherosclerosis, IL-6 deficiency on an E$^{-/-}$ background has no effect when mice were killed at 16 weeks of age (25, 26). However, IL-6 through IL-6ST mediates the production of IL-12, and the latter when deficient on the E$^{-/-}$ background results in decreased atherosclerosis (27). IL-6ST is shared by many cytokines that act through JAK–STAT pathways, including IL-6, IL-11, ciliary neurotrophic factor, leukemia inhibitory factor, oncostatin M, cardiotrophin-1, and cardiotrophin-like cytokine (28). Several of these cytokines, e.g., oncostatin M, have been linked to atherosclerosis or other types of cardiovascular diseases. Increased expression of IL-6ST in combination with elevated levels of circulating IL-6 in A20$^{+/-}$ mice might result in deregulation of IL-6-gp130 signaling, leading to altered inflammatory responses and subsequent development of atherosclerosis.

NF-κB activation also mediates the expression of genes that are clearly antiinflammatory, such as the cytokine IL-10. The effect of IL-10 on atherogenesis has been studied extensively with different mouse models, all of which demonstrated that IL-10 is an antiatherogenic factor (29–31). Accordingly, the raised IL-10 plasma levels in A20-haploinsufficient mice may also protect against lesion formation. Because pro atherogenic (IL-1β, IL-12p40), ambiguous (IL-6), and antiatherogenic (IL-10) cytokines are all increased in plasma of A20-haploinsufficient mice, their net effect or an imbalance between proinflammatory and antiinflammatory cytokines might increase atherosclerosis susceptibility.

A recent analysis of SNPs linked variability in the human A20 gene to the risk of coronary artery disease (CAD) in type 2 diabetes, a condition characterized by chronic NF-κB activation. Two tag SNPs were independently associated with CAD in two groups of patients. In both groups, the minor allele was affiliated with lower levels of A20 mRNA in blood mononuclear cells and predisposition to CAD, and the major allele was affiliated with higher A20 mRNA levels and protection against CAD. To explain this association, it was speculated that lower A20 expression may predispose to CAD by permitting NF-κB to remain more active and consequently leading to increased expression of

downstream atherogenic mediators (32). This idea is compatible with what has been presented here.

The results presented here suggest that A20 might not be the culprit gene in the atherosclerosis susceptibility locus on mouse chromosome 10. In the quantitative trait locus analysis the genotypic means for the marker at the peak logarithm of odds score indicated that homozygosity for the FVB allele resulted in a 2-fold increase in atherosclerosis over mice that are either heterozygotes or homozygotes for the B6 allele (1). We previously showed that the FVB form of A20 is more potent at shutting down NF-κB activity than the B6 form (6). Therefore, if A20 was the responsible gene at the chromosome 10 locus, based on these experiments one would predict homozygosity for the FVB allele to be associated with less, not more, atherosclerosis. One caveat of this conclusion is that our studies determining the relative activities of FVB-A20 and B6-A20 were done in transfected 293 and vascular smooth muscle cells, whereas in the current study A20 in lesions was localized mainly to endothelial cells and lipid-laden macrophages. Although unlikely, it is possible that A20 mediates different functions (antiapoptotic vs. NF-κB activation) in these cell types so that in sum the FVB form could be proatherogenic (33, 34). Thus it will be necessary to study cell type-specific conditional knockdown of A20 before entirely excluding it as the responsible atherosclerosis susceptibility gene at the chromosome 10 locus.

Materials and Methods

Creation of A20 Tg Mice and Origin of A20-Haploinsufficient Mice. The BAC 146-P3, which only contains the A20 gene, was obtained from a mouse ES BAC library (Genome Systems, St. Louis) generated from the 129SV/J strain, which has A20 is identical to the FVB strain. It consists of mouse chromosome 10 18,690,335 to 18,704,826 base pairs cloned into the pBelo vector. This BAC was introduced by pronuclear microinjection into B6-fertilized eggs and founder B6.tg(A20) mice were backcrossed two generations to B6.ApoE$^{-/-}$ mice (stock no. 002052; Jackson Laboratory, Bar Harbor, ME) to obtain B6.ApoE$^{-/-}$tg(A20) mice. Mice were screened for the presence of the A20 containing BAC by PCR of genomic DNA. Expression of the transgene was demonstrated by using a PCR that only amplified the 129SV/J-FVB form of A20. In tg mouse liver expression of 129SV/J-FVB A20 was $\approx$4-fold higher than in nontransgenic mouse liver (data not shown). The primer sequences used for these PCRs are provided in supporting information (SI) Table 1. A20-haploinsufficient (A20$^{+/-}$) mice on a mixed background were kindly provided by Averil Ma from the University of California, San Francisco. These mice were backcrossed to B6.ApoE$^{-/-}$ mice by a marker-assisted technique through five generations (>99% B6) to obtain B6.ApoE$^{-/-}$.A20$^{+/-}$ mice (1).

Atherosclerosis Studies in A20-Haploinsufficient and A20 Tg Mice. For atherosclerosis studies in A20-haploinsufficient mice B6.ApoE$^{-/-}$.A20$^{+/-}$ and B6 ApoE$^{-/-}$ mice were intercrossed, and offspring with two (A20$^{+/+}$) and one (A20$^{+/-}$) intact copies of the A20 gene were compared. For studies in A20-overexpressing mice, B6.ApoE$^{-/-}$tg(A20) mice were crossed with FVB.ApoE$^{-/-}$ mice, and F_1 offspring with and without the A20 transgene were compared. All mice used for atherosclerosis studies were weaned at 28 days of age onto a semisynthetic modified AIN76a diet containing 0.02% cholesterol (35). Mice were killed at 16 weeks of age after a 6-h fast with free access to water. They were exsanguinated by left-ventricular puncture, and blood was collected into EDTA-containing syringes. The circulation was flushed with PBS, and the heart was removed and stored frozen in Tissue-Tek OCT compound (B6.ApoE$^{-/-}$A20$^{+/+}$ and A20$^{+/-}$ hearts) or in buffered formalin [F_1.ApoE$^{-/-}$tg(A20) and F_1 hearts] (35). The animals were housed in the Rockefeller University Laboratory Animal Research Center under a protocol approved by the Institutional Animal Care and Use Committee in a specific pathogen-free environment in rooms with a light-dark cycle.

Blood Analysis. Lipoprotein fractions from 60 μl of plasma were isolated by sequential ultracentrifugation in a TL-100 ultracentrifuge (Beckman Coulter, Fullerton, CA). Cholesterol was determined enzymatically by a colorimetric method (Roche, Indianapolis, IN) in the original plasma sample (total cholesterol) and the 1.063 g/ml infranatant (high-density lipoprotein cholesterol). Circulating cytokine levels of IL-1β, IL-6, IL-10, IL-12 (p40), and TNF-α were determined by using a multiplex suspension ELISA (Bio-Rad, Hercules, CA). Standard curves for each cytokine were generated ranging from 2 to 8,000 pg/ml. Undiluted plasma samples (50 μl) were incubated with 50 μl of antibody-coupled microsphere sets (5,000 beads per cytokine per well) for 1 h at room temperature and processed as recommended by the supplier (Bio-Rad). Concentrations of cytokines were read on a Bioplex Protein Array System (Bio-Rad).

Quantification of Atherosclerosis. To quantify atherosclerosis at the aortic root, formalin-fixed or OCT-embedded hearts were sectioned and stained with oil red O as described (18). While all sections were used to quantify atherosclerosis in formalin fixed hearts, for OCT-embedded hearts every other section was saved for immunohistochemistry.

Immunostaining. Frozen sections of the aortic root were fixed in ice-cold acetone (10 min) and washed with PBS. Peroxidases were quenched with 1% H_2O_2 (10 min). Sections were washed and blocked with 5% normal serum (goat serum for CD68 and CD31, sheep serum for α-actin, and donkey serum for A20) for 20 min. Primary antibodies were incubated for 90 min [anti CD68/MAC 1957 GA (rat), 1:100 dilution, Serotec (Raleigh, NC); anti-CD31 (PECAM) (rat), 1:10 dilution, BD Pharma (Franklin Lakes, NJ); anti actin IgG (rabbit), 1:80 dilution, Biomedical Technologies, Stoughton, MA; and anti TNF-aip3 (chicken), 1:100 dilution, Abcam, Cambridge, MA]. Sections were washed and incubated with HRP-conjugated secondary antibody for 30 min (goat anti-rat IgG/HRP, STAR 72, 1:50 dilution for CD68 and CD31, Serotec; sheep anti-rabbit IgG/HRP STAR54, 1:50 dilution for actin and donkey anti-chicken IgG, Serotec; and 1:500 dilution for TNF-aip3 Jackson ImmunoResearch, West Grove, PA). After washing, peroxidase was visualized by incubation with Nova Red (Vector Laboratories, Burlingame, CA), and sections were counterstained with hematoxylin. Sections were dried and permanently mounted with VectaMount mounting medium (Vector Laboratories). Aortic root sections were stained for TUNEL-positive cells by using the *In Situ* Cell Death Detection Kit from Roche following the manufacturer's instructions. Movat pentachrome, which is a general connective tissue stain that stains elastic fibers black, collagen fibers yellow, proteoglycans blue or green, and smooth muscle cells red was used to determine the overall composition of lesions.

RNA Isolation. RNA was isolated from tissue samples by using the TRIzol reagent (Invitrogen, Carlsbad, CA) according to the manufacturer's protocol. To remove contaminating DNA, the DNA-free kit from Ambion (Austin, TX) was used. cDNA was generated from total RNA with the SUPERSCRIPT II Rnase H$^-$ Reverse Transcriptase Kit (Invitrogen) using 1–2 μg of total RNA as template and a 1:1 mixture of oligo(dT) and hexamer primers. The resulting cDNA pool was used for radioactive RT-PCR or *Taq*Man analysis.

Radioactive RT-PCR/*Taq*Man. The cDNA pools provided templates for radioactive PCRs using specific primers at annealing tem-

peratures between 60°C and 65°C in the presence of dNTPs, [α-^{32}P]dCTP, and *Taq*DNA polymerase. Expression of the A20-BAC transgene was quantified by strain-specific PCR screening using liver cDNA pools from A20 tg mice and controls. A difference in the annealing temperature between B6-A20 and 129/FVB-A20 was introduced by use of a short 3′ end primer that contained the A20-coding SNP at its 3′ end and allowed us to screen for A20 BAC expression. The Sequence Detection System 7700 (Applied Biosystems, Boston, MA) was used for amplification and specific sequence detection. Forward and reverse PCR primers were used at a final concentration of 300 nM, and probes, containing a 5′ fluorophor (6-FAM) and a 3′ quencher (TAMRA), were used at a final concentration of 100 nM. Cycling parameters were: 2 min 50°C, 10 min 95°C and 40 times: 30 s 95°C, 1 min 65°C. Primers were purchased from Sigma (St. Louis, MO) and probes were from Applied Biosystems. The primer sequences used for PCR are provided in SI Table 1.

PIQOR Microarrays Technology. Forty micrograms of liver RNA was isolated from five individual B6.ApoE$^{-/-}$.A20$^{+/-}$ and A20$^{+/+}$ male mice. The resultant 200 μg of pooled RNA was labeled with FluoroLink Cy3-dCTP (Amersham Pharmacia Biotech, Piscataway, NJ) (A20$^{+/-}$) or FluoroLink Cy5-dCTP (Amersham Pharmacia Biotech) (A20$^{+/+}$) during cDNA synthesis according to the manufacturer's instructions. Labeled cDNA pools were cleaned, combined, and hybridized to PIQOR immunology, mouse-sense microarrays (kind gift from Miltenyi Biotec, Bergisch Gladbach, Germany) following the manufacturer's instructions. The experiment was repeated twice with the same set of animals.

Statistical Analysis. All data are expressed as mean ± SEM unless indicated otherwise. Distributions were tested for normality, and statistical analysis was done by *t* test for normally and by Mann–Whitney test for not-normally distributed data by using Prism software, version 4.0.

1. Dansky HM, Shu P, Donavan M, Montagno J, Nagle DL, Smutko JS, Roy N, Whiteing S, Barrios J, McBride TJ, *et al.* (2002) *Genetics* 160:1599–1608.
2. Teupser D, Tan M, Persky AD, Breslow JL (2006) *Proc Natl Acad Sci USA* 103:123–128.
3. Krikos A, Laherty CD, Dixit VM (1992) *J Biol Chem* 267:17971–17976.
4. Opipari AW, Jr, Boguski MS, Dixit VM (1990) *J Biol Chem* 265:14705–14708.
5. Lee EG, Boone DL, Chai S, Libby SL, Chien M, Lodolce JP, Ma A (2000) *Science* 289:2350–2354.
6. Idel S, Dansky HM, Breslow JL (2003) *Proc Natl Acad Sci USA* 100:14235–14240.
7. Boone DL, Turer EE, Lee EG, Ahmad RC, Wheeler MT, Tsui C, Hurley P, Chien M, Chai S, Hitotsumatsu O, *et al.* (2004) *Nat Immunol* 5:1052–1060.
8. Kaminska B (2005) *Biochim Biophys Acta* 1754:253–262.
9. Cybulsky MI, Gimbrone MA, Jr (1991) *Science* 251:788–791.
10. Iiyama K, Hajra L, Iiyama M, Li H, DiChiara M, Medoff BD, Cybulsky MI (1999) *Circ Res* 85:199–207.
11. Nakashima Y, Raines EW, Plump AS, Breslow JL, Ross R (1998) *Arterioscler Thromb Vasc Biol* 18:842–851.
12. Cybulsky MI, Iiyama K, Li H, Zhu S, Chen M, Iiyama M, Davis V, Gutierrez-Ramos JC, Connelly PW, Milstone DS (2001) *J Clin Invest* 107:1255–1262.
13. Dansky HM, Barlow CB, Lominska C, Sikes JL, Kao C, Weinsaft J, Cybulsky MI, Smith JD (2001) *Arterioscler Thromb Vasc Biol* 21:1662–1667.
14. Brach MA, Henschler R, Mertelsmann RH, Herrmann F (1991) *Pathobiology* 59:284–288.
15. Rajavashisth T, Qiao JH, Tripathi S, Tripathi J, Mishra N, Hua M, Wang XP, Loussararian A, Clinton S, Libby P, Lusis A (1998) *J Clin Invest* 101:2702–2710.
16. Smith JD, Trogan E, Ginsberg M, Grigaux C, Tian J, Miyata M (1995) *Proc Natl Acad Sci USA* 92:8264–8268.
17. Schreyer SA, Vick CM, LeBoeuf RC (2002) *J Biol Chem* 277:12364–12368.
18. Branen L, Hovgaard L, Nitulescu M, Bengtsson E, Nilsson J, Jovinge S (2004) *Arterioscler Thromb Vasc Biol* 24:2137–2142.
19. Ohta H, Wada H, Niwa T, Kirii H, Iwamoto N, Fujii H, Saito K, Sekikawa K, Seishima M (2005) *Atherosclerosis* 180:11–17.
20. Kirii H, Niwa T, Yamada Y, Wada H, Saito K, Iwakura Y, Asano M, Moriwaki H, Seishima M (2003) *Arterioscler Thromb Vasc Biol* 23:656–660.
21. Chi H, Messas E, Levine RA, Graves DT, Amar S (2004) *Circulation* 110:1678–1685.
22. Michelsen KS, Wong MH, Shah PK, Zhang W, Yano J, Doherty TM, Akira S, Rajavashisth TB, Arditi M (2004) *Proc Natl Acad Sci USA* 101:10679–10684.
23. Mullick AE, Tobias PS, Curtiss LK (2005) *J Clin Invest* 115:3149–3156.
24. Bjorkbacka H, Kunjathoor VV, Moore KJ, Koehn S, Ordija CM, Lee MA, Means T, Halmen K, Luster AD, Golenbock DT, Freeman MW (2004) *Nat Med* 10:416–421.
25. Elhage R, Clamens S, Besnard S, Mallat Z, Tedgui A, Arnal J, Maret A, Bayard F (2001) *Atherosclerosis* 156:315–320.
26. Huber SA, Sakkinen P, Conze D, Hardin N, Tracy R (1999) *Arterioscler Thromb Vasc Biol* 19:2364–2367.
27. Davenport P, Tipping PG (2003) *Am J Pathol* 163:1117–1125.
28. Heinrich PC, Behrmann I, Haan S, Hermanns HM, Muller-Newen G, Schaper F (2003) *Biochem J* 374:1–20.
29. Caligiuri G, Rudling M, Ollivier V, Jacob MP, Michel JB, Hansson GK, Nicoletti A (2003) *Mol Med* 9:10–17.
30. Mallat Z, Besnard S, Duriez M, Deleuze V, Emmanuel F, Bureau MF, Soubrier F, Esposito B, Duez H, Fievet C, *et al.* (1999) *Circ Res* 85:e17–e24.
31. Von Der Thusen JH, Kuiper J, Fekkes ML, De Vos P, Van Berkel TJ, Biessen EA (2001) *FASEB J* 15:2730–2732.
32. Boonyasrisawat W, Eberle D, Bacci S, Zhang YY, Nolan D, Gervino EV, Johnstone MT, Trischitta V, Shoelson SE, Doria A (2007) *Diabetes* 56:499–505.
33. Daniel S, Arvelo MB, Patel VI, Longo CR, Shrikhande G, Shukri T, Mahiou J, Sun DW, Mottley C, Grey ST, Ferran C (2004) *Blood* 104:2376–2384.
34. Patel VI, Daniel S, Longo CR, Shrikhande GV, Scali ST, Czismadia E, Groft CM, Shukri T, Motley-Dore C, Ramsey HE, *et al.* (2006) *FASEB J* 20:1418–1430.
35. Teupser D, Persky AD, Breslow JL (2003) *Arterioscler Thromb Vasc Biol* 23:1907–1913.